Generalized Monte Carlo loop algorithm for two-dimensional frustrated Ising models

Yuan Wang and Hans De Sterck
Department of Applied Mathematics, University of Waterloo, Ontario, N2L 3G1, Canada

Roger G. Melko
Department of Physics and Astronomy, University of Waterloo, Ontario, N2L 3G1, Canada

(Received 2 August 2011; published 13 March 2012)

We introduce a generalized loop move (GLM) update for Monte Carlo simulations of frustrated Ising models on two-dimensional lattices with bond-sharing plaquettes. The GLM updates are designed to enhance Monte Carlo sampling efficiency when the system's low-energy states consist of an extensive number of degenerate or near-degenerate spin configurations, separated by large energy barriers to single spin flips. Through implementation on several frustrated Ising models, we demonstrate the effectiveness of the GLM updates in cases where both degenerate and near-degenerate sets of configurations are favored at low temperatures. The GLM update's potential to be straightforwardly extended to different lattices and spin interactions allows it to be readily adopted on many other frustrated Ising models of physical relevance.

DOI: 10.1103/PhysRevE.85.036704 PACS number(s): 02.70.−c, 05.50.+q, 75.10.Hk, 05.10.−a

I. INTRODUCTION

Monte Carlo (MC) simulations are among the most ubiquitous computational tools used in statistical physics and material science. Modern MC methods, evolved from the original Metropolis algorithm of the 1950s [1], have become increasingly sophisticated with the advent of cluster moves, histogram reweighting methods, parallel tempering, and other technical advances [2]. This sophistication, coupled with the continuing increase in available computing power, allows MC methods to simulate classical and quantum statistical mechanical systems of a level of complexity unimaginable even a decade ago. Indeed, the remarkable growth in the size of systems accessible to MC simulations is owed as much to the advancement of algorithm technology as it is to the increase in available raw CPU power through Moore's law [3].

Lattice magnetic systems offer some of the greatest challenges to MC practitioners. In fact, it was realized early on that MC simulations of the ferromagnetic Ising model employing simple local updates [single spin flip (SSF) algorithms] suffer severe critical slowing down—a rapid increase in autocorrelation times—near a second-order phase transition. This stimulated work on nonlocal (cluster or collective-mode) algorithms, such as the well-known Swendsen-Wang [4] and Wolff [5] algorithms. A different situation that also requires nonlocal updates is known to occur in broad classes of frustrated magnetic Ising models. Such models, typically identified by predominantly antiferromagnetic (AFM) or random interactions, can have disordered ground states, which consist of an extensive number of equal-energy (degenerate) spin configurations—such is famously the case for the triangular lattice Ising model with AFM interactions [6,7]. In such models, simple SSF updates have the tendency to bring the configuration out of the degenerate manifold of ground states, hence costing an energy proportional to the Ising interaction. At sufficiently low temperatures, the Metropolis algorithm will reject such moves, inhibiting *ergodicity*, which is the ability of the MC simulation to explore the entire degenerate manifold of states in reasonable (i.e., nonexponential) computing time.

This issue was recently brought to the forefront in the broad class of *ice* or *vertex* models [8–10]. Of largest interest are the so-called *spin ice* models [11]—Ising models on a frustrated pyrochlore lattice, which are realized experimentally in some rare-earth titanate compounds. Ideal spin ice Ising models promote a disordered degenerate ground state. However, it was found that weak perturbations, such as occur from long-range dipolar interactions, can energetically favor one or several configurations [12]. Exploration of different configurations contributing to the degenerate ground state is thus a crucial task for MC simulations, and can be efficiently achieved through loop updates [13]. The behavior of loops in spin ice and related models is also intimately tied to important physical phenomena such as the Kasteleyn transition [14] and the concept of fluctuations between topologically ordered ground-state sectors [15,16].

Since the identification of loop algorithms is topical not only as a simulation technique but as a probe into the physics of materials, it is remarkable that generalized loop algorithms do not exist for broad classes of different frustrated models. Rather, each system typically needs to have an algorithm designed based on the particular constraints of its ground-state manifold. Such is the case for vertex models [10], spin ice [13,17] (and related corner-sharing triangle models such as the Ising kagome AFM), the fully frustrated square lattice Ising model [18], the fully frustrated honeycomb Ising model [19], and others [20,21]. In the present work, we address this shortcoming by introducing a generalized loop algorithm for a large class of frustrated Ising models with bond-sharing plaquettes.

The paper is organized as follows. In Sec. II, we outline the generalized loop move (GLM) update in detail for a class of two-dimensional frustrated Ising models, illustrating the specific examples of the triangular lattice Ising AFM, and the fully frustrated square and honeycomb lattice Ising models. We prove rigorously that the algorithm obeys detailed balance (Appendix), and demonstrate explicitly that it reproduces the results expected in traditional MC simulations of these models (Sec. III A). In Sec. III B, we simulate extensions of the models, perturbed by weakening one bond per plaquette (an interaction that can arise experimentally, e.g., in frustrated magnets when

uniaxial pressure is applied [15]). In this case, the GLM update vastly outperforms traditional single-spin flips in the exploration of the low-temperature physics of the models, in particular in finding a unique ordered ground state. As discussed in Sec. IV, GLM updates will help open the way for the efficient simulation of a wide range of frustrated magnetic models in the future.

II. GENERALIZED LOOP ALGORITHM FOR ISING MODELS

A. Ising models

We consider classical Ising models that have Hamiltonians of the general form

$$H = \sum_{\langle i,j \rangle} J_{ij}\delta_{ij} S_i^z S_j^z, \tag{1}$$

where spin variables S_i^z can take the value of $\pm 1/2$. In this paper, we refer to *unperturbed* models as those with J_{ij} equal to a constant $J > 0$, while *perturbed* models (discussed in Sec. III B) have some of the $J_{ij} = J' \neq J$ (but still positive). The bond variables δ_{ij} are defined to have a value of either $+1$ ("AFM") or -1 ("FM") for each bond on the lattice. In a given spin configuration, a bond is referred to as *satisfied* if $\delta_{ij} S_i^z S_j^z < 0$ and *unsatisfied* otherwise. An Ising model is referred to as *frustrated* if it is impossible for any spin configuration to satisfy all of the bonds on the lattice. We consider both perturbed and unperturbed versions of the following two-dimensional (2D) periodic lattice models in this paper (Fig. 1):

(1) The triangular lattice AFM, where all $\delta_{ij} = 1$.
(2) The fully frustrated square lattice.
(3) The fully frustrated honeycomb lattice.

For the latter two lattices, uniform AFM interactions are unfrustrated; full frustration can be induced by enforcing the constraint that the product of the sign of the bond variables around *each* closed plaquette (square or hexagon) satisfies

$$\prod_{ij \in \text{plaq}} \delta_{ij} = -1, \tag{2}$$

e.g., $\delta_{ij} = -1$ for one bond, and $\delta_{ij} = 1$ for the rest. Since each plaquette is frustrated such interactions are called *fully frustrated* (FF). Thus defined, the three unperturbed frustrated Ising models that we are considering are known to have disordered ground states with an extensive number of equal-energy configurations [6,7,22–24]. The geometry of the FM and AFM bonds for each lattice is illustrated in Fig. 1.

B. Single-spin flips

It is common to study the finite temperature (T) and ground-state properties of such models using Markov chain Metropolis Monte Carlo methods. Traditionally, single spin flip (SSF) updates are employed in the Monte Carlo algorithm; one simply attempts to flip a single spin (one at a time) by computing the corresponding change in energy (ΔE) and then accepting the update with a Metropolis condition using probability:

$$P_{\text{flip}} = \min(1, e^{-\Delta E/T}). \tag{3}$$

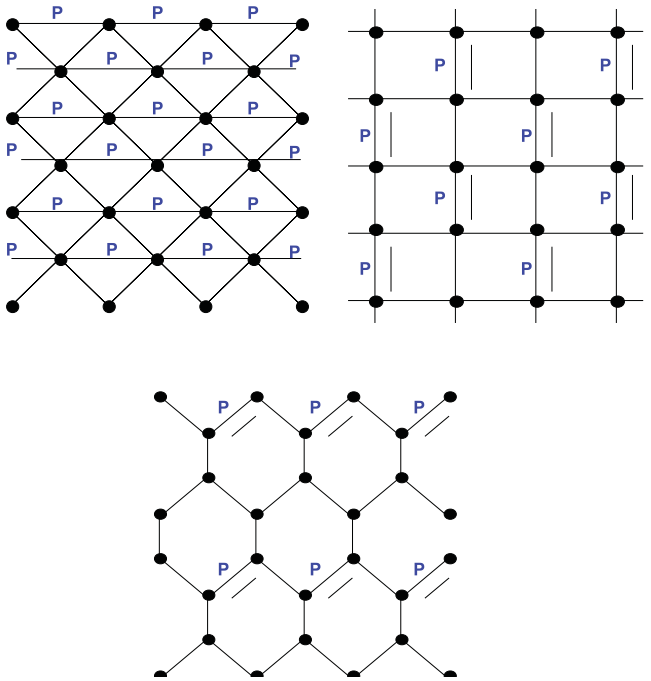

FIG. 1. (Color online) Frustrated Ising spin models: AFM triangle (top left), FF square (top right), and FF honeycomb (bottom). The single bonds represent AFM bonds, the double bonds represent FM bonds, and the perturbed (weakened) bonds in the perturbed Ising models are indicated by "P" (see Sec. III B).

In frustrated Ising models, many spin configurations are local energy minima, and most SSF attempts cost a large energy proportional to J. Based on Eq. (3), the probability of accepting such a SSF update decreases exponentially as the temperature decreases. Consequently, at $T \ll J$, once a SSF simulation has reached one of the local energy minima it is very unlikely for the simulation to accept any SSF updates. As a result, SSF updates tend to become "frozen" into one of the local energy minima at $T \ll J$ (i.e., ergodicity is lost).

One can observe that in these local energy minima, there are often groups of spins that could be flipped together without changing the number of unsatisfied bonds (and hence without significantly changing the energy of the system). Cluster algorithms take advantage of this observation to find and flip such groups of spins [10].

C. Generalized loop move

Motivated by the above, we introduce a generalized loop move (GLM) algorithm. The GLM is designed to complement single spin flips, in a way that improves the sampling of equal (or nearly equal) energy configurations near the ground states of 2D periodic frustrated Ising models with bond sharing plaquettes. Like previous algorithms designed to work on specific Ising models [10,12,19], the GLM algorithm is designed to work by finding clusters of spins that could be flipped together *without* changing the number of unsatisfied bonds, and then attempting to flip them. If we take a cluster of spins in the lattice, we can call the bonds that are adjacent to one spin inside the cluster and one spin outside the cluster "boundary bonds" (see Fig. 2 for illustration). It can be

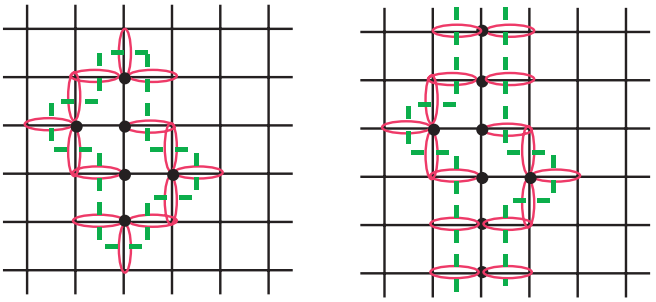

FIG. 2. (Color online) The figure on the left shows a nonspanning cluster of spins and the figure on the right shows a spanning cluster of spins. The spins inside the cluster are represented by the large dots and the boundary bonds are circled. The thick dashed line shows the simple cycles in the dual lattice that are dual to the boundary bonds. We will call the simple cycle on the left figure a closed loop because it encloses a cluster of spins. We will call the simple cycles on the right figure cuts because each simple cycle individually does not enclose a cluster of spin.

observed that when a cluster of spins are flipped, the previously unsatisfied boundary bonds become satisfied (and vice versa), while the other bonds are unaffected. Therefore to find a cluster of spins that could be flipped without changing the number of unsatisfied bonds, we can look for a cluster of spins bounded by an equal number of satisfied and unsatisfied bonds. Furthermore, if we consider the dual lattice to the spin lattice, defined in the usual graph theory sense, the subset of dual edges that are dual to the boundary bonds form one or a pair of simple cycles in the dual lattice (taking into account the periodicity of the lattices). The GLM algorithm takes advantage of these observations to find a desired cluster of spins, by finding simple cycles in the dual lattice that are dual to an equal number of satisfied and unsatisfied bonds. To simplify this process, the GLM algorithm is constrained to finding simple cycles in the dual lattice that are alternatingly dual to satisfied and unsatisfied bonds. Note the following intricacies in this approach:

1. Perturbed lattice models, or models with bonds of different strength: While the GLM does not change the number of unsatisfied bonds, it can change the energy of the spin system, depending on the strength of the bonds being made satisfied and unsatisfied. At low temperatures, even small increases in energy would be strongly inhibited. To overcome this difficulty, a weighting scheme is introduced to favor dual edges dual to strong unsatisfied bonds and weak satisfied bonds for inclusion in the simple cycle. This increases the likelihood of finding a random cluster of spins that is energetically favored to be flipped. Empirical testing has shown that GLM updates with the weighting scheme are much more efficient at equilibriating perturbed Ising models at low temperature (and finding the true ground state) than GLM algorithm without the weighting scheme.

2. Periodic boundary conditions: Due to the periodic nature of the lattice, some clusters of spins will wrap around the spin lattice. The boundary bonds for such spin clusters are dual to a pair of simple cycles in the dual lattice. For some perturbed Ising models at low temperatures, it is observed that these clusters are often the only ones that are energetically favored to be flipped. To enable the GLM algorithm to find these clusters, whenever the first simple cycle wraps around the spin lattice and deleting the bonds dual to the simple cycle does not partition the spin lattice into two, the GLM algorithm will attempt to find a second simple cycle. If deleting the bonds dual to the pair of simple cycles partitions the spin lattice, then the GLM algorithm has successfully found the desired spin cluster. Otherwise, the GLM attempt is aborted.

The GLM algorithm is described in detail in the following section.

D. Algorithm description

The GLM algorithm is designed to supplement SSFs. Therefore in each Monte Carlo iteration, SSF is first attempted on each spin in the lattice followed by a fixed number of attempts of GLM. In this paper, the authors chose to use $N/30$ attempts (where N is the number of spins in the lattice). In each GLM attempt, the algorithm performs the following procedure:

1. Find a simple cycle in the dual lattice that is alternatingly dual to satisfied and unsatisfied bonds in the spin lattice

Begin by randomly selecting a dual node in the dual lattice. Call the subset of dual edges adjacent to the dual node E. Randomly select one of the dual edges in E based on the following weighting scheme:

$$W(B_{ij}) = \begin{cases} e^{\alpha\beta[|J_{ij}|-\text{Mean}_{B_{kl}\in E}(|J_{kl}|)]} & \text{if} \quad B_{ij} \text{ is unsatisfied,} \\ e^{-\alpha\beta[|J_{ij}|-\text{Mean}_{B_{kl}\in E}(|J_{kl}|)]} & \text{if} \quad B_{ij} \text{ is satisfied.} \end{cases} \tag{4}$$

Note: the $\alpha > 0$ in Eq. (4) above determines the strength with which the weighting scheme favors strong unsatisfied bonds and weak satisfied bonds. Through empirical observation, $\alpha = 5$ is found to work well and it is used in the numerical results section of this paper.

Go to the other dual node adjacent to the selected dual edge. Consider the dual edges adjacent to it that meet the following conditions:

(i) If the last dual edge added to the chain is dual to a satisfied bond, then only consider dual edges that are dual to unsatisfied bonds, and vice versa.

(ii) Exclude dual edges that will complete a nonalternating cycle if added to the chain.

If this subset is empty, then abort the algorithm. Otherwise, randomly select a dual edge from this subset based on the same weighting scheme described in Eq. (4). Go to the other dual node adjacent to the selected dual edge and continue the process described above until the algorithm encounters a dual node already in the chain completing the simple cycle.

2. Partition the spin lattice into two sublattices

If deleting all the bonds dual to the simple cycle found above partitions the spin lattice into two sublattices, then the algorithm will use this partitioning of the spin lattice. Otherwise, repeat the algorithm described in the previous subsection to find a second simple cycle. If deleting all the bonds dual to the pair of simple cycles partitions the spin lattice into two sublattices, then the algorithm will use this

partitioning of the spin lattice. Otherwise, the algorithm aborts the GLM attempt.

3. Attempt to flip all the spins in the smaller sublattice

Once the spin lattice is partitioned into two sublattices, the algorithm should flip all the spins in the smaller sublattice with probability $P_{\text{accept}}()$ defined below. For ease of exposition, the following notation and definitions are established:

(i) Let $f(C)$ be a function that takes a chain of dual edges C that is alternatingly dual to satisfied and unsatisfied bonds ("alternating chain") and ends in a simple cycle and reverses the order of dual edges that are part of the simple cycle. This is illustrated in Fig. 3. Function f is used in the definition of acceptance probability because if C is an alternating chain under spin configuration S_1, then $f(C)$ is an alternating chain under under the new spin configuration after flipping all the spins inside the simple cycle.

(ii) Let $P_{\text{select}}(C)$ be the probability of the GLM algorithm encountering a particular chain of dual edges C as it tries to find a simple cycle. Note: To compute $P_{\text{select}}(C)$, one must simply multiply together the probability of each of the stochastic choices made during the chain-building steps that resulted in the particular chain being constructed.

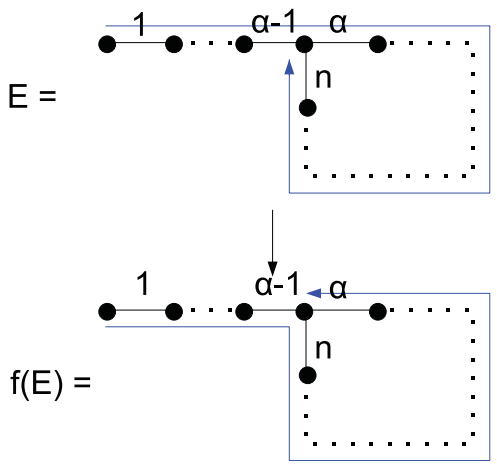

FIG. 3. (Color online) This figure shows how the function F reverses the order of dual edges in the loop.

(iii) Let S_1 denote the current spin configuration, and let S_2 denote the spin configuration if all the spins in the smaller sublattice are flipped.

If the partition boundary is found with one chain C, then

$$P_{\text{accept}}(C,\, S_1) = \min\left[1,\, e^{-\beta[E(S_2)-E(S_1)]}\,\frac{P_{\text{select}}(f(C),\, S_2)}{P_{\text{select}}(C,\, S_1)}\right]. \tag{5}$$

If the partition boundary is found with two chains C_1 and C_2, then

$$P_{\text{accept}}((C_1,\, C_2),\, S_1) = \min\left[1,\, e^{-\beta[E(S_2)-E(S_1)]}\,\frac{P_{\text{select}}(f(C_1),\, S_2)\,P_{\text{select}}(f(C_2),\, S_2)}{P_{\text{select}}(C_1,\, S_1)\,P_{\text{select}}(C_2,\, S_1)}\right]. \tag{6}$$

Note when the lattice is unperturbed, $E(S_1) = E(S_2)$. A rigorous proof of detailed balance is included in the Appendix.

III. SIMULATION RESULTS

In this section we examine some typical data from Monte Carlo simulations of three frustrated Ising models, using simulations with SSF and GLM updates. In Sec. III A, thermodynamic data for unperturbed Ising models are compared between simulations employing only SSF, and simulations using both SSF and GLM updates. Some GLM loop properties are characterized. In Sec. III B, we examine the performance of the GLM updates on the three perturbed Ising models, which are constructed to have a finite-T phase transition to a ground state with a unique spin configuration. We demonstrate that GLM updates help the simulation find the correct ground state in cases where SSF updates alone fail.

A. Results on unperturbed models

Metropolis Monte Carlo simulations are performed on the three aforementioned Ising models: AFM triangular, FF square, and FF honeycomb (Fig. 1). A typical run employs an *annealing* technique where the simulation is started at a high temperature ($T = 0.5$), and T is gradually lowered through small steps until the system settles in its disordered degenerate ground state. At each temperature, equilibriation is performed, then a fixed number of iterations of either SSF or a combination of SSF and GLM is applied and measurement estimators such as energy and magnetization are collected. Each annealing simulation is performed twice for comparison: once with SSF only, and once with a combination of SSF and GLM updates.

The first numerical result we consider is the internal energy of the Ising models under an annealing simulation. As illustrated in Fig. 4, the internal energy measured as a function of temperature appears identical between SSF and GLM simulations, to within statistical error. This lends practical proof to the fact that the GLM updates are "well behaved" (do not disrupt detailed balance in the Monte Carlo procedure), and find the same degenerate manifold of states as the SSF updates alone. In addition to annealing simulations, we also tested the performance of SSF and GLM in *quenched simulations* where the entire simulation (including the equilibriation period) is run at a single temperature. We ran these single simulations at $T = 0.05$, finding that for the case of the AFM triangular and FF square lattice Ising models, both SSF and GLM were able to find a ground-state configuration, the efficiency gain through GLM not being significant in this case. However, for the FF honeycomb lattice, SSF simulations tend to be noticeably slow in finding the disordered ground state, a situation remedied by employing GLM updates. This difficulty for SSF alone to simulate the low-temperature thermodynamic behavior of the FF honeycomb lattice was

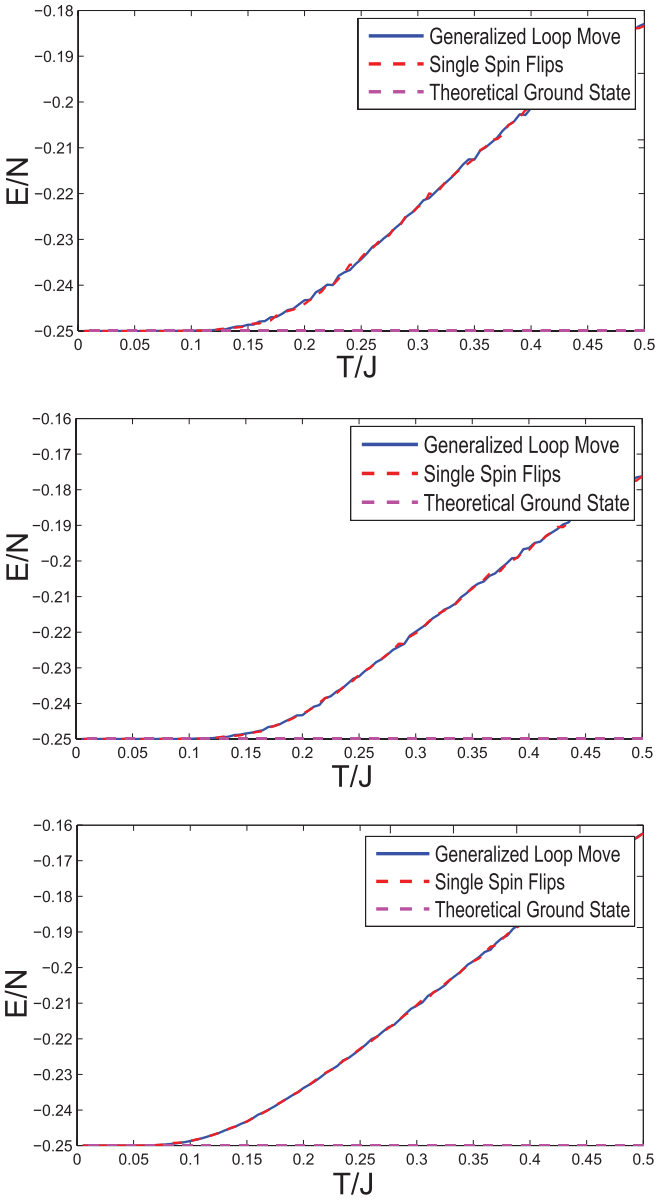

FIG. 4. (Color online) Energy per spin (E/N) for the AFM triangular lattice (top), FF square lattice (middle), and FF honeycomb lattice (bottom). The theoretical true ground-state energy per spin for each system is -0.25.

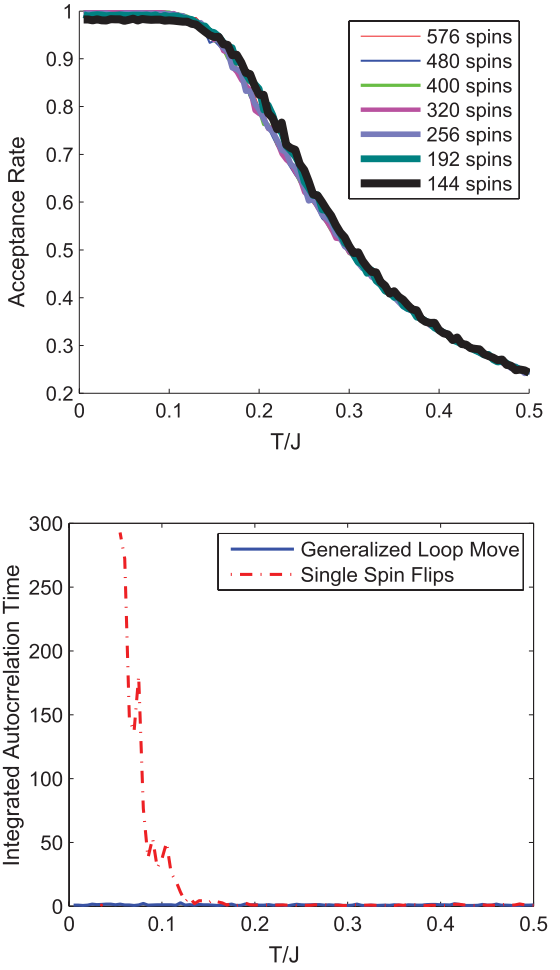

FIG. 5. (Color online) The acceptance rate of GLM updates on the AFM triangular lattice (top). At bottom, the integrated autocorrelation time for the magnetization squared on the FF honeycomb lattice with 144 spins.

also noted in the work by Andrews *et al.* [19] where a cluster update specific to the FF honeycomb was proposed. In Andrews' work, it was shown that in an annealing simulation, SSF alone tends to become frozen in one of the ground states at low temperatures, which is evident by the inability of the average magnetization to converge to zero, seen in Fig. 3(c) of Ref. [19]. On the other hand, both the algorithm proposed in Ref. [19] and GLM updates can find the correct average magnetization through annealing or quenched simulations.

A meaningful characterization of the low-temperature dynamics of the GLM updates can be determined via the study of the acceptance rate of the algorithm. We define the acceptance rate as the percentage of GLM attempts that result in *successful* group spin flips. For the AFM triangular lattice (shown in Fig. 5), the acceptance rate increases as temperature decreases and appears independent of lattice size. For the FF square lattice (not shown), the acceptance rate is high across the whole temperature range and appears to approach unity as lattice size increases. For the FF honeycomb lattice, the acceptance rate is high across the temperature range, increasing as the temperature decreases, and apparently increasing with lattice size. Most importantly, the fact that the acceptance rate is large (of order unity) in all cases, particularly for $T/J \leqslant 0.1$, suggests that the GLM updates are successful in exploring the manifold of degenerate configurations that contribute to the disordered ground state. This is in direct contrast to a simulation employing SSF updates only, which has exponentially suppressed acceptance rates for $T \ll J$.

We also examine autocorrelation functions, defined for a Monte Carlo time series of observables $\mathcal{O}(1)$, $\mathcal{O}(2)$,..., by the normalized correlation function,

$$A[\mathcal{O}](t) = \frac{\langle \mathcal{O}(i+t)\mathcal{O}(i)\rangle - \langle \mathcal{O}(i)\rangle^2}{\langle \mathcal{O}(i)^2\rangle - \langle \mathcal{O}(i)\rangle^2}, \tag{7}$$

where the averages are over the Monte Carlo "time" steps i (iterations in the Markov chain). Higher autocorrelations imply that produced samples are less independent. We define

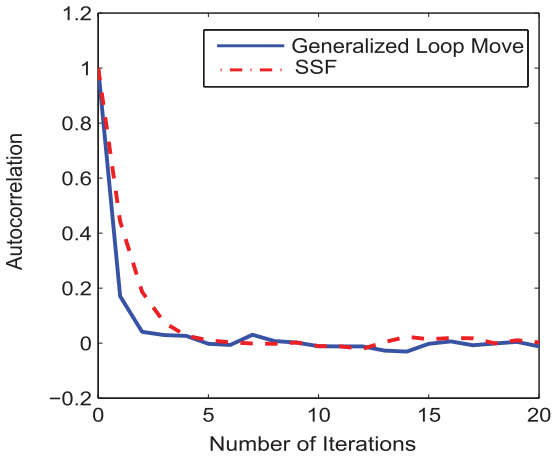

FIG. 6. (Color online) Autocorrelation function [Eq. (7)] for magnetization squared on the FF triangle lattice with 144 spins at $T = 0.1$.

the integrated autocorrelation time as

$$\tau_{\text{int}}[\mathcal{O}] = \frac{1}{2} + \sum_{t=1}^{\infty} A[\mathcal{O}](t), \tag{8}$$

using as the observable $\mathcal{O}$. Figure 5 compares the integrated autocorrelation times for the FF honeycomb lattice model. Here, the SSF displays diverging integrated autocorrelations below $T \approx 0.1$, whereas in contrast GLM integrated autocorrelations remain relatively low. For the FF square and AFM triangle lattices, the integrated autocorrelation does not diverge at low temperatures for both SSF and GLM. At higher temperatures, autocorrelation functions for SSF and GLM updates can appear almost identical (Fig. 6).

The average number of dual edges that the GLM algorithm encounters in each successful attempt of the GLM (which we will call *chain* size) and the average number of dual edges that form the partition boundary (which we will call *loop* size) provide a measure of the amount of work that the GLM algorithm needs to perform in each iteration. How these two values change with temperature and system size is of interest in determining the efficiency of the algorithm. As illustrated in Fig. 7, for the unperturbed FF square lattice model, the loop

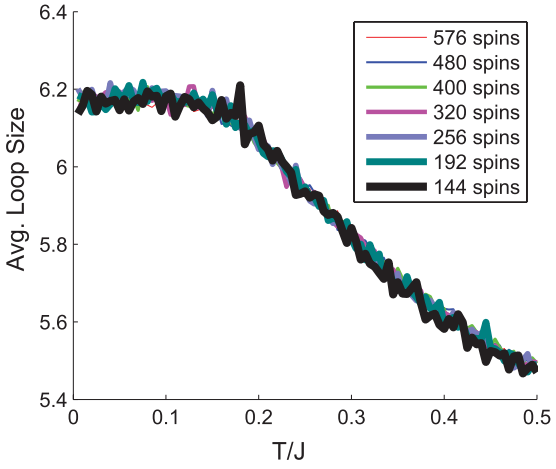

FIG. 7. (Color online) Loop size for the FF square lattice.

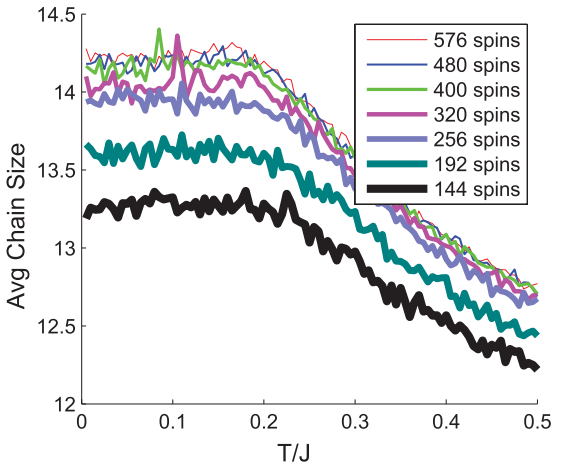

FIG. 8. (Color online) Chain size for the FF square lattice.

size is independent of lattice size, and increases slightly as temperature decreases. As illustrated in Fig. 8, the chain size also appears to increase as temperature decreases. The chain size tends to increase with lattice size, approaching a limit for large lattices. The increase in chain size with lattice size for smaller systems is likely due to a finite-size effect, meaning that for large lattices both chain size and loop size will saturate. Similar results are also observed for the loop size and chain size on AFM triangle and FF honeycomb lattices. This suggests that the work performed in each GLM attempt is proportional to a fixed multiple of the work performed in each SSF update on a single spin. This computational complexity of the GLM attempt is the motivation behind each GLM iteration consisting of one SSF sweep followed by $N/30$ GLM attempts[1] in this paper. In this way, the work performed in each GLM iteration is expected to be comparable to a fixed multiple of the work performed in a SSF sweep. More rigorous study would be required to confirm this expected computational complexity of the GLM algorithm.

B. Results on perturbed models

We now explore the effect of anisotropy in the Ising interaction on the performance of the MC algorithm, with SSF and GLM updates. In the following, we define perturbed Ising models by weakening one bond per plaquette in Eq. (1), where two different strengths of J_{ij} are used: J and J'. The location of weakened bonds are defined via the geometry illustrated in Fig. 1. The one weakened bond per plaquette has the strength $J'/J = 0.9$. In the AFM triangular case, $\delta_{ij} = 1$ for all bonds, and weakened bonds are chosen arbitrarily to occur along all rows of the lattice; in the two FF models, the weakened bond is chosen to correspond to the FM bond with $\delta_{ij} = -1$ for simplicity. In each case, the degenerate manifold of ground states is lifted resulting in two unique ground states (related by symmetry) where the unsatisfied bonds occur uniquely at the perturbed bond locations. This perturbation presents a greater difficulty for SSF MC algorithms to accurately compute

[1]This number was found to provide a good balance between SSF and GLM updates on the models studied.

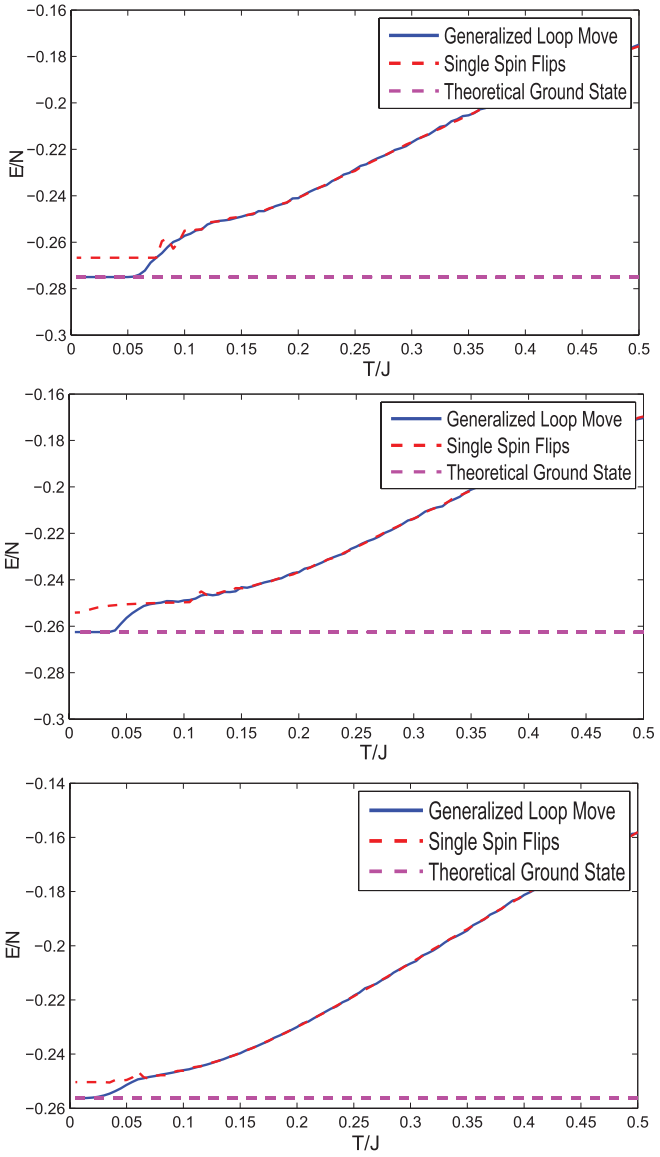

FIG. 9. (Color online) Energy per spin for the perturbed AFM triangular lattice (top), perturbed FF square lattice (middle), and perturbed FF honeycomb lattice (bottom).

low-temperature statistics, and find the true ground state. As illustrated in Fig. 9, SSF updates are unable to find the true ground-state energy in any of the three perturbed Ising models through an annealing procedure. GLM updates, on the other hand, are able to find the true ground state through annealing (as well as in quenched simulations run at a single temperature $T \ll J$). It is interesting to note that at low temperatures, the internal energy curve for GLM is noticeably smoother than the internal energy curve for SSF alone. This suggests that GLM is able to converge to equilibrium faster than SSF alone.

As can be seen in Fig. 10, for the perturbed FF honeycomb lattice model, the acceptance rate of GLM updates increases as the temperature decreases between $T = 0.5$ and 0.1, and then sharply drops off to zero below $T = 0.1$. This abrupt drop to zero corresponds to the finite-T phase transition that occurs in these models at a temperature proportional to the perturbed energy scale, which the GLM updates are able to

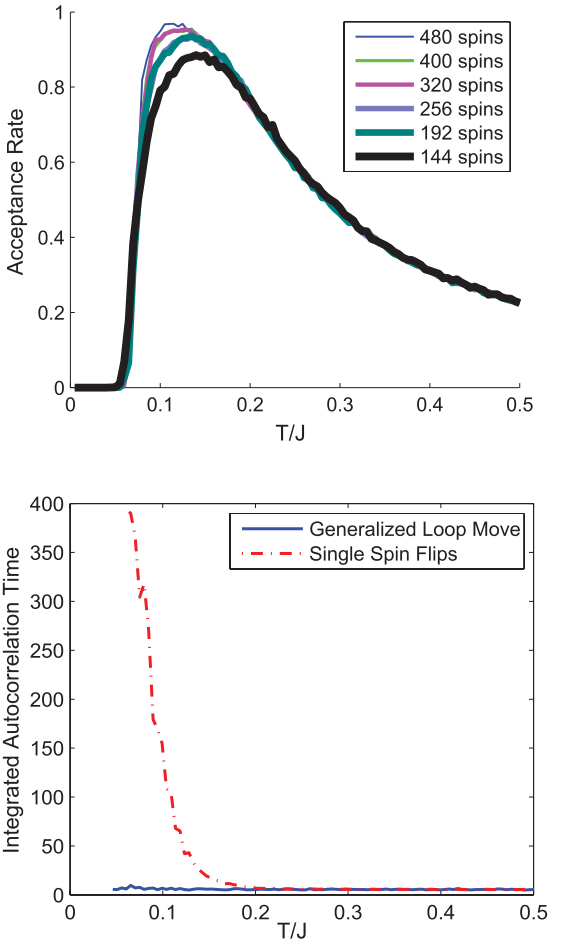

FIG. 10. (Color online) The acceptance rate of GLM updates on the perturbed FF honeycomb lattice (top). At bottom, the integrated autocorrelation time results of magnetization squared for the perturbed FF honeycomb lattice with 144 spins.

find cleanly. Integrated autocorrelation times show a clear difference between SSF and GLM updates (Fig. 10). An example of the autocorrelation function for the energy is shown in Fig. 11, which clearly indicates that GLM moves are better at producing independent samples at that particular temperature.

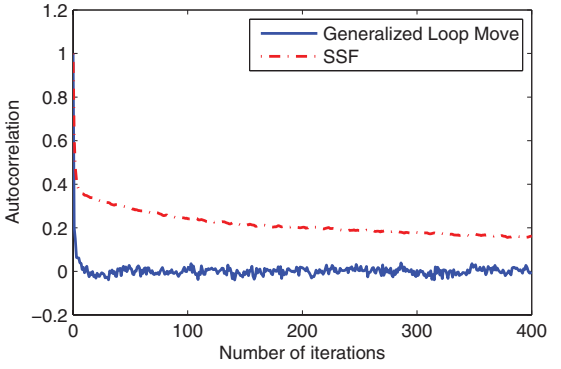

FIG. 11. (Color online) Autocorrelation function [Eq. (7)] for energy on the perturbed FF honeycomb lattice with 144 spins at $T = 0.1$.

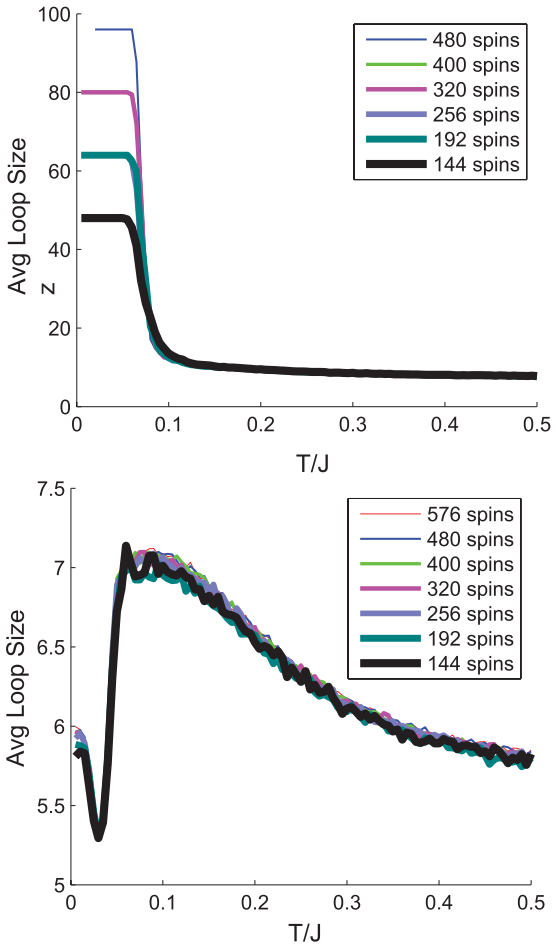

FIG. 12. (Color online) Loop size for the perturbed AFM triangular lattice (top) and perturbed FF honeycomb lattice (bottom).

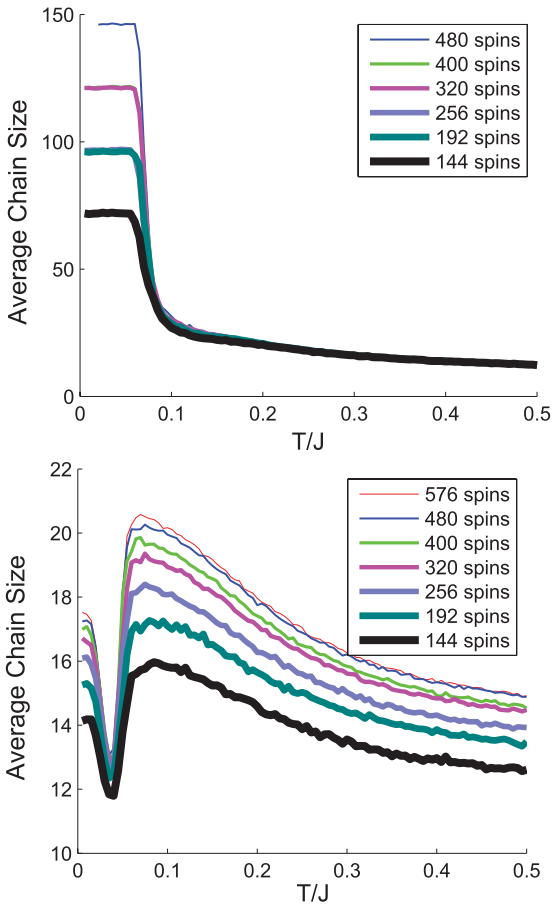

FIG. 13. (Color online) Chain size for the perturbed AFM triangular lattice (top) and perturbed FF honeycomb lattice (bottom).

For the case of perturbed Ising models, temperature has a significant effect on loop and chain size. For perturbed AFM triangle (Fig. 12) and FF square lattices (not illustrated), at high temperatures ($T = 0.5$–0.1) loop size appears independent of lattice size but at low temperatures (below the phase transition) loop size grows linearly with the shortest side of the lattice. This is expected based on observing GLM updates in action. For perturbed AFM triangle and FF square lattices at low temperatures, the GLM algorithm tends to encounter spin configurations where the only possible partition boundaries are those that wrap around the lattice. For the perturbed FF honeycomb lattice, loop size appears independent of lattice size regardless of temperature. As illustrated in Fig. 13, chain size behaves similar to loop size with respect to lattice size and temperature, with the exception of finite-size effects at small lattice sizes. These results on loop size and chain size suggest that in the ground state of some perturbed Ising models (such as AFM triangle and FF square) the amount of work the GLM algorithm needs to perform in each GLM attempt will grow linearly with size of the lattice at low temperatures. This implies that the amount of work done in each GLM iteration (one SSF iteration followed by x attempts of the GLM where $x = N/30$) will grow quadratically with system size at low temperatures. This expensive algorithm cost can be avoided in practical situations by recognizing it as a sign of the underlying long-range order of the system—extensive sampling by the GLM update is not necessary in such a case. Regardless, further simulation results would be required to determine the computational complexity of the GLM update in this interesting case.

IV. DISCUSSION

In this paper, we have presented a generalized loop move (GLM) update for a class of frustrated Ising models on two-dimensional lattices which are composed of bond-sharing plaquettes. The algorithm is designed to allow efficient Metropolis Monte Carlo updates in a degenerate or quasidegenerate set of spin configurations that contribute to an extensive manifold of disordered low-energy states. We have thoroughly described the algorithm with the goal of making it easy to implement in a wide variety of models, and have provided a rigorous proof of detailed balance in the general case.

We implemented and tested the algorithm on three prototypical lattice models, the antiferromagnetic triangular-lattice Ising model, and the fully frustrated square- and honeycomb-lattice Ising models. All three models admit a disordered, extensively degenerate manifold of configurations in their unperturbed ground state. The GLM update is demonstrated to complement traditional single spin-flip updates in allowing the simulation to find all configurations that contribute to the degenerate manifold at low temperatures. In contrast to single

spin flips, the GLM update is able to sample configurations in the degenerate subspace with a very high acceptance rate, which is independent of temperature for $T \ll J$. The GLM achieves this while maintaining a very efficient $O(N)$ complexity for each N-site lattice.

Perturbing the models by weakening one bond per plaquette (triangle, square, or hexagon) causes them to select a unique spin configuration in their ground state. Although single spin-flip updates typically cannot find this unique state due to the large energy barriers associated with sampling the quasi-degenerate manifold of states, we have shown that the GLM updates are capable of computing the correct low-temperature statistics, as well as finding the equilibrium ground state in a highly efficient manner.

We expect that our current work in describing and characterizing the GLM updates will lead to their use in other frustrated Ising spin models of physical importance. The GLM algorithm, as described in this paper, can be straightforwardly generalized to work on other frustrated Ising models on two-dimensional lattices of bond-sharing plaquettes. It would be interesting to explore the effectiveness of the GLM update on models where the exchange J_{ij} is randomly frustrated, such as Edwards-Anderson spin glass models [25]. Finally, we expect that the GLM moves will be particularly useful in simulations of more realistic models of frustrated materials, where additional long-range interactions, local perturbations, or pressure-induced interaction anisotropy leads to the selection of a unique ground state.

ACKNOWLEDGMENTS

We thank S. Inglis and G. Sanders for many useful discussions. This work was made possible by the facilities of the Shared Hierarchical Academic Research Computing Network (SHARCNET) and Compute/Calcul Canada. Support was provided by NSERC of Canada.

APPENDIX: PROOF OF DETAILED BALANCE

To prove detailed balance, we need to show that given any two spin configurations S_1 and S_2, the following equation is satisfied:

$$\Pi(S_1)T(S_1 \to S_2) = \Pi(S_2)T(S_2 \to S_1), \tag{A1}$$

where $\Pi(S)$ denotes the Boltzmann probability of spin configuration S, and $T(S_i \to S_j)$ denote the transition probability in the generalized loop move algorithm from spin configuration S_i to spin configuration S_j.

1. Preliminary notations and definitions

For ease of exposition, it is convenient to establish the following notations and definitions:

(1) Let Γ be the set of all possible dual edge chains that step 1 of the GLM algorithm can generate (i.e., Γ is the set of dual edge chains that are alternatingly dual to satisfied and unsatisfied bonds and end in a simple cycle).

(2) Take any two spin configurations S_1 and S_2, and let

(a) $\Gamma_1 = \{\gamma \in \Gamma |\ \gamma$ end in a closed loop (e.g., Fig. 2) and flipping all the spins inside the closed loop takes the spin system from S_1 to $S_2\}$,

(b) $\Omega_1 = \{(\gamma_1,\gamma_2) \in (\Gamma \times \Gamma) | \gamma_1,\gamma_2$ end in cuts L_1, L_2 (e.g., Fig. 2); flipping all the spins inside $L_1 \cup L_2$ takes the spin system from S_1 to $S_2\}$,

(c) $\Psi_1 = \Gamma_1 \cup \Omega_1$,

(d) $\Gamma_2 = \{\gamma \in \Gamma |\ \gamma$ end in a closed loop and flipping all the spins inside the closed loop takes the spin system from S_2 to $S_1\}$,

(e) $\Omega_2 = \{(\gamma_1,\gamma_2) \in (\Gamma \times \Gamma) | \gamma_1,\gamma_2$ end in cuts L_1, L_2 and flipping all the spins inside $L_1 \cup L_2$ takes the spin system from S_2 to $S_1\}$,

(f) $\Psi_2 = \Gamma_2 \cup \Omega_2$,

(g) $\Psi_1^{'} = \{\psi \in \Psi_1 |\ P_{\text{accept}}(\psi, S_1) > 0\}$ where P_{accept} is defined as in Eqs. (5) or (6),

(h) $\Psi_2^{'} = \{\psi \in \Psi_2 |\ P_{\text{accept}}(\psi, S_2) > 0\}$ where P_{accept} is defined as in Eqs. (5) or (6).

($\Psi_1^{'}$ and $\Psi_2^{'}$ are defined as above to facilitate the proof of detailed balance.)

(3) Define F: $\Gamma \cup (\Gamma \times \Gamma) \to \Gamma \cup (\Gamma \times \Gamma)$ such that $F(\gamma) = f(\gamma)\ \forall \gamma \in \Gamma$ and $F((\gamma_1,\gamma_2)) = (f(\gamma_1), f(\gamma_2))\ \forall (\gamma_1,\gamma_2) \in (\Gamma \times \Gamma)$.

(4) Let $\tilde{F}$ be the restriction of F to $\Psi_1^{'}$ For convenience, we will also define $P_{\text{select}}((\gamma_1,\gamma_2), S) = P_{\text{select}}(\gamma_1, S) P_{\text{select}}(\gamma_2, S)\ \forall (\gamma_1,\gamma_2) \in (\Gamma \times \Gamma)$.

Note: $T(S_i \to S_j) = \sum_{\psi \in \Psi_i^{'}} P_{\text{select}}(\psi, S_i) P_{\text{accept}}(\psi, S_i)$, where $(i, j) = (1, 2)$ or $(2, 1)$.

2. Proof of detailed balance

If we can prove the following three subclaims:

(1) $\tilde{F}(\Psi_1^{'}) \subseteq \Psi_2^{'}$ (this is used to prove subclaim 2),

(2) $\tilde{F}$ is bijective between $\Psi_1^{'}$ and $\Psi_2^{'}$,

(3) $\forall \psi \in \Psi_1^{'}$, $\Pi(S_1) P_{\text{select}}(\psi, S_1) P_{\text{accept}}(\psi, S_1) = \Pi(S_2) P_{\text{select}}(\tilde{F}(\psi), S_2) P_{\text{accept}}(\tilde{F}(\psi), S_2)$,

then, the proof for detailed balance follows naturally:

$$\sum_{\psi \in \Psi_1^{'}} \Pi(S_1) P_{\text{select}}(\psi, S_1) P_{\text{accept}}(\psi, S_1) = \sum_{\psi \in \Psi_1^{'}} \Pi(S_2) P_{\text{select}}(\tilde{F}(\psi), S_2) P_{\text{accept}}(\tilde{F}(\psi), S_2)$$

by subclaim 3

$$\Rightarrow \quad \sum_{\psi \in \Psi_1^{'}} \Pi(S_1) P_{\text{select}}(\psi, S_1) P_{\text{accept}}(\psi, S_1) = \sum_{\delta \in \Psi_2^{'}} \Pi(S_2) P_{\text{select}}(\delta, S_2) P_{\text{accept}}(\delta, S_2)$$

because $\tilde{F}$ is bijective between $\Psi_1^{'}$ and $\Psi_2^{'}$

$$\Rightarrow \quad \Pi(S_1) \sum_{\psi \in \Psi_1^{'}} P_{\text{select}}(\psi, S_1) P_{\text{accept}}(\psi, S_1) = \Pi(S_2) \sum_{\delta \in \Psi_2^{'}} P_{\text{select}}(\delta, S_2) P_{\text{accept}}(\delta, S_2)$$

$$\Rightarrow \quad \Pi(S_1) T(S_1 \to S_2) = \Pi(S_2) T(S_2 \to S_1).$$

3. Proof of subclaims

Subclaim 1: $\tilde{F}(\Psi_1') \subseteq \Psi_2'$

Take any $\psi \in \Psi_1'$, show that $\tilde{F}(\psi) \in \Psi_2'$.

(1) $\tilde{F}(\psi) \in \Psi_2$ because

(a) $\psi \in \Psi_1$ implies that ψ ends in a closed loop or union of complementary cuts that forms a partition boundary around a group of spins that if flipped will take the spin configuration from S_1 to S_2. Therefore $\tilde{F}(\psi)$ ends in a closed loop or union of complementary cuts that forms a partition boundary around the same group of spins, which if flipped will take the spin configuration from S_2 back to S_1;

(b) and $P_{\text{select}}(\tilde{F}(\psi), S_2) > 0$ because

$$\begin{aligned}\psi \in \Psi_1' &\Rightarrow P_{\text{accept}}(\psi, S_1) > 0 \\ &\Rightarrow \min\left(1, e^{-\beta[E(S_2)-E(S_1)]}\frac{P_{\text{select}}(\tilde{F}(\psi), S_2)}{P_{\text{select}}(\psi, S_1)}\right) > 0 \\ &\Rightarrow P_{\text{select}}(\tilde{F}(\psi), S_2) > 0,\end{aligned}$$

(2) $P_{\text{accept}}(\tilde{F}(\psi), S_2)$

$$= \min\left(1, e^{-\beta[E(S_2)-E(S_1)]}\frac{P_{\text{select}}(\psi, S_1)}{P_{\text{select}}(\tilde{F}(\psi), S_2)}\right) > 0$$

because $\psi \in \Psi_1' \subseteq \Psi_1 \Rightarrow P_{\text{select}}(\psi, S_1) > 0$.

(3) 1 & 2 $\Longrightarrow \tilde{F}(\psi) \in \Psi_2'$. Therefore $\tilde{F}(\Psi_1') \subseteq \Psi_2'$.

Subclaim 2: $\tilde{F}$ ***is bijective between*** Ψ_1' ***and*** Ψ_2'

(1) $\tilde{F}$ is injective because $\tilde{F}(\Psi_1') \subseteq \Psi_2'$ by subclaim 1 and take any $\psi_1, \psi_2 \in \Psi_1$, $\tilde{F}(\psi_1) = \tilde{F}(\psi_2) \Rightarrow \psi_1 = \psi_2$ by definition of $f()$;

(2) $\tilde{F}$ is surjective because for any $\delta \in \Psi_2'$, $F(\delta) \in \Psi_1'$ by subclaim 1, and $\tilde{F}(F(\delta)) = \delta$.

Subclaim 3: For any $\boldsymbol{\psi \in \Psi_1'}$***, show that***

$$\boldsymbol{\Pi(S_1)P_{\text{select}}(\psi, S_1)P_{\text{accept}}(\psi, S_1) = \Pi(S_2)P_{\text{select}}(\tilde{F}(\psi), S_2)P_{\text{accept}}(\tilde{F}(\psi), S_2).}$$

Let $a = \Pi(S_1)P_{\text{select}}(\psi, S_1)$, and $b = \Pi(S_2)P_{\text{select}}(\tilde{F}(\psi), S_2)$. Then,

$$\begin{aligned}\Pi(S_1)P_{\text{select}}(\psi, S_1)P_{\text{accept}}(\psi, S_1) &= \Pi(S_1)P_{\text{select}}(\psi, S_1)\min\left(1, \frac{\Pi(S_2)}{\Pi(S_1)}\frac{P_{\text{select}}(\tilde{F}(\psi), S_2)}{P_{\text{select}}(\psi, S_1)}\right) \\ &= a\ \min\left(1, \frac{b}{a}\right) \\ &= \min(a, b), \\ \Pi(S_2)P_{\text{select}}(\tilde{F}(\psi), S_2)P_{\text{accept}}(\tilde{F}(\psi), S_2) &= \Pi(S_2)P_{\text{select}}(\tilde{F}(\psi), S_2)\min\left(1, \frac{\Pi(S_1)}{\Pi(S_2)}\frac{P_{\text{select}}(\psi, S_1)}{P_{\text{select}}(\tilde{F}(\psi), S_2)}\right) \\ &= b\ \min\left(1, \frac{a}{b}\right) \\ &= \min(a, b).\end{aligned}$$

Therefore $\Pi(S_1)P_{\text{select}}(\psi, S_1)P_{\text{accept}}(\psi, S_1) = \Pi(S_2)P_{\text{select}}(\tilde{F}(\psi), S_2)P_{\text{accept}}(\tilde{F}(\psi), S_2)$.

[1] N. Metropolis, A. W. Rosenbluth, M. N. Rosenbluth, A. H. Teller, and E. Teller, J. Chem. Phys. **21**, 1087 (1953).

[2] J. Liu, *Monte Carlo Strategies in Scientic Computing* (Springer, New York, 2001).

[3] G. E. Moore, Electronics **38**, 8 (1965).

[4] R. H. Swendsen and J.-S. Wang, Phys. Rev. Lett. **58**, 86 (1987).

[5] U. Wolff, Phys. Rev. Lett. **62**, 361 (1989).

[6] G. H. Wannier, Phys. Rev. **79**, 357 (1950).

[7] R. M. F. Houtappel, Physica **16**, 425 (1950).

[8] H. G. Evertz, G. Lana, and M. Marcu, Phys. Rev. Lett. **70**, 875 (1993).

[9] H. G. Evertz, Adv. Phys. **52**, 1 (2003).

[10] G. T. Barkema and M. E. J. Newman, Phys. Rev. E **57**, 1155 (1998).

[11] S. T. Bramwell and M. J. P. Gingras, Science **294**, 1495 (2001).

[12] R. G. Melko, B. C. den Hertog, and M. J. P. Gingras, Phys. Rev. Lett. **87**, 067203 (2001).

[13] H. Shinaoka and Y. Motome, Phys. Rev. B **82**, 134420 (2010).

[14] L. D. C. Jaubert, J. T. Chalker, P. C. W. Holdsworth, and R. Moessner, Phys. Rev. Lett. **100**, 067207 (2008).

[15] L. D. Jaubert, J. Chalker, P. C. Holdsworth, and R. Moessner, Phys. Rev. Lett. **105**, 087201 (2010).

[16] A. J. Macdonald, P. C. W. Holdsworth, and R. G. Melko, J. Phys.: Condens. Matter **23**, 164208 (2011).

[17] M. Orendáč, J. Hanko, E. Čižmár, A. Orendáčová, M. Shirai, and S. T. Bramwell, Phys. Rev. B **75**, 104425 (2007).

[18] D. Kandel, R. Ben-Av, and E. Domany, Phys. Rev. Lett. **65**, 941 (1990).

[19] S. Andrews, H. De Sterck, S. Inglis, and R. G. Melko, Phys. Rev. E **79**, 041127 (2009).

[20] D. Kandel and E. Domany, Phys. Rev. B **43**, 8539 (1991).

[21] P. D. Coddington and L. Han, Phys. Rev. B **50**, 3058 (1994).

[22] M. E. Fisher, Phys. Rev. **124**, 1664 (1961).

[23] R. Moessner and S. L. Sondhi, Phys. Rev. B **63**, 224401 (2001).

[24] W. F. Wolff and J. Zittartz, Z. Phys. B **49**, 129 (1982).

[25] I. Bieche, R. Maynard, R. Rammal, and J. P. Uhry, J. Phys. A **13**, 2553 (1980).